HAL
open science

POST SEISMIC DEFORMATION FOLLOWING THE APRIL 25,2015 GORKHA EARTHQUAKE: AFTERSLIP VERSUS VISCOUS RELAXATION.

François Jouanne, Ananta Prasad Gajurel, Jean-Louis Mugnier, Laurent Bollinger, Lok Bijaya Adhikari, Bharat Koirala, Nathalie Cotte, Roshanraj Bhattarai, Arnaud Pecher, Pascale Bascou, et al.

▶ To cite this version:

François Jouanne, Ananta Prasad Gajurel, Jean-Louis Mugnier, Laurent Bollinger, Lok Bijaya Adhikari, et al.. POST SEISMIC DEFORMATION FOLLOWING THE APRIL 25,2015 GORKHA EARTHQUAKE: AFTERSLIP VERSUS VISCOUS RELAXATION.. Journal of Asian Earth Sciences, 2019, 10.1016/j.jseaes.2019.02.009 . hal-02395962

HAL Id: hal-02395962

https://hal.science/hal-02395962v1

Submitted on 5 Oct 2022

HAL is a multi-disciplinary open access archive for the deposit and dissemination of scientific research documents, whether they are published or not. The documents may come from teaching and research institutions in France or abroad, or from public or private research centers.

L'archive ouverte pluridisciplinaire **HAL**, est destinée au dépôt et à la diffusion de documents scientifiques de niveau recherche, publiés ou non, émanant des établissements d'enseignement et de recherche français ou étrangers, des laboratoires publics ou privés.

POSTSEISMIC DEFORMATION FOLLOWING THE APRIL 25, 2015 GORKHA EARTHQUAKE: AFTERSLIP VERSUS VISCOUS RELAXATION.

François Jouanne (1), Ananta Gajurel (2), Jean-Louis Mugnier (1), Laurent Bollinger (3), Lok Bijaya Adhikari (4), Bharat Koirala (4), Nathalie Cotte (1), Roshanraj Bhattarai (2,1), Arnaud Pecher (1), Pascale Bascou (1), Pascale Huyghe (1).

1Univ. Grenoble Alpes, Univ. Savoie Mont Blanc, CNRS, IRD, IFSTTAR, ISTerre.
2 Department of Geology, Tribhuvan University, Ghantaghar, Kathmandu, Nepal
3 CEA, DAM, DIF, Arpajon, France.
4 Department of Mines and Geology, National Seismological Center, Kathmandu, Nepal.

Received in original form: 8 July 2017.

Abbreviated title suitable for page headings:
Postseismic deformation following the Gorkha earthquake.

Corresponding author:
François Jouanne,
Université de Savoie Mont Blanc, ISTerre,
F-73376 Le Bourget du Lac, France
Email : fjoua@univ-smb.fr
Tel : (33)608371432

SUMMARY.

. The postseismic deformation consecutive to the April 25, 2015 Gorkha earthquake (7.8 Mw) is estimated in this paper based on a cGNSS network installed prior to the earthquake and supplemented by cGNSS stations installed after the main shock. Postseismic velocities are obtained from recorded velocities corrected for interseismic deformation and seasonal variations . The maximum postseismic displacement is found north of the rupture area, and locally reached 100 mm between the earthquake and late 2016. The postseismic deformation extends in the northern part of the rupture area whereas there is a lack of postseismic deformation south of the rupture, along the southern part of the Main Himalayan Thrust. Three hypotheses for the mechanisms controlling postseismic deformation are tested through numerical simulations of the postseismic time series: viscous relaxation, afterslip or a combination of these two mechanisms. We can exclude postseismic deformation controlled by viscous relaxation of a thick deformation zone along the northern and lower flat of the MHT. However, it is not possible to discriminate between postseismic deformation controlled by either an afterslip along the MHT (northern part of the rupture zone, crustal ramp and lower flat of the MHT) or a combination of afterslip along the MHT (northern part of the rupture zone, crustal ramp) and viscous relaxation along a thin (~3km thick) low viscosity body centered on the lower flat of the MHT.

Keywords:

Creep and deformation, Transient deformation, Asia, Seismic cycle, Space geodetic surveys.

INTRODUCTION.

The April 25, 2015 Mw 7.8 Gorkha earthquake provides a unique opportunity to study a large Himalayan earthquake with continuous GNSS data (Avouac et al., 2015), InSAR investigations (e.g. Grandin et al., 2015) and good seismological data (Adhikari et al., 2015; Baillard et al., 2017). The implementation of a cGNSS network, prior to the earthquake, has also allowed to quantify the early postseismic surface deformation consecutive to this large earthquake (Mencin et al., 2016).

The 2015 earthquake (Fig. 1) is a very good example to study the complexity of the seismic cycle in a continental subduction zone: it indicates that the convergence along a main thrust is consumed during various types of earthquakes (Mugnier et al., 2013), some of which partially contributes to release the elastic strain of the Main Himalayan Thrust (Avouac et al., 2015). This partial release has already been instrumentally measured in several oceanic subduction environments; for example, in the Andean convergent margin, the main slip patch of the 2010 Mw 8.8 earthquake occurred in an area that was highly coupled and had already released slip in 1960 (Melnick et al., 2012; Moreno et al., 2012). However, the 2015 Gorkha event provides a unique opportunity to study the postseismic deformation: in an oceanic subduction zone, GNSS data cannot be deployed in the marine area located above the rupture whereas 12 stations were located all around the Gorkha rupture zone. Furthermore, during the weeks following the main shock, the dataset has been completed by the deployment of other permanent or semi-permanent GNSS stations (this paper).

Nonetheless, the mechanism controlling the postseismic deformation associated with the 2015 Gorka event has not yet been studied in detail. Different mechanisms are usually inferred for the postseismic deformation: afterslip or viscous relaxation. Given that the coseismic displacement field for this earthquake has been estimated (e.g. Avouac, 2015) and the geometry of the Main Himalayan Thrust is rather well imaged (Duputel et al., 2016), it is possible to numerically simulate the GNSS time series illustrating the postseismic deformation in order to

determine the mechanisms controlling this deformation in Nepal. The Relax software (Barbot et al., 2009) was used to model the postseismic deformation and three mechanisms have been tested: afterslip, viscous relaxation or a combination of these two phenomena. We used a flap-ramp-flat geometry (Elliott et al., 2016) with a southern and upper flat corresponding to the geometry adopted by Grandin et al. (2016) to describe the coseismic slip distribution of the Gorkha earthquake along this flat.

GEOLOGICAL SETTING.

The structure of the Himalaya results from the underthrusting of the Indian lithosphere along the Main Himalayan Thrust (MHT) beneath the Tibetan Plateau (Argand, 1924). Great earthquakes have episodically ruptured segments of the brittle upper part of the MHT (e.g. Avouac et al., 2001; Mugnier et al., 2013). The Nepal earthquake of April 25, 2015 followed a series of great earthquakes in Central Himalaya (Mugnier et al., 2011; Bollinger et al., 2014): over the last two centuries, the city of Kathmandu was severely damaged in 1833, 1866, 1934. The April 25, 2015 event (Fig. 1) is the first event that occurred along the MHT and which was simultaneously recorded by numerous instruments: high-rate GPS (e.g. Avouac et al., 2015), teleseismic waves (e.g. Fan and Shearer, 2015), SAR imaging (e.g. Lindsey et al., 2015), InSAR and teleseismic waves (Grandin et al., 2016), strong-motion recordings (e.g. Bhattarai et al., 2015) and a local seismometer network (Adhikari et al., 2015).

Commenté [p1]: Pas dans la biblio

Commenté [p2]: Pas dans la biblio

The rupture was mainly located to the NW of Kathmandu, at a depth of 13-15 km on a flat portion of the Main Himalayan Thrust (MHT) that dips towards the N-NE by 7-10°. The northern boundary of the main rupture corresponds to the transition towards a steeper crustal ramp. This ramp, which is partly coupled during the interseismic period (Jouanne et al., 2017), is only locally affected by the earthquake (Elliott et al., 2016). The southern boundary of the rupture was near the leading edge of the Lesser Himalaya antiformal duplex (Mugnier et al.,

2017) and possibly near the frontal footwall ramp of the upper Nawakot duplex (Hubbard et al., 2016). This rupture was affected by transversal structures: on the western side, a ~20° dipping lateral ramp (Kumar et al., 2017), located beneath the Judi lineament (Mugnier et al., 2017) and already defined by Kayal (2008), separates the main rupture zone from the nucleation area. On the eastern side, a lateral ramp (Mugnier et al., 2017) located beneath the Gaurishankar lineament (Kayal, 2008) separates the April 25, 2015 rupture from the May 12, 2015 (Mw 7.2) rupture.

DATA ACQUISITION AND ANALYSIS.

After the April 25 Gorkha earthquake, we installed a GNSS network designed to record postseismic deformation induced by this Mw 7.8 earthquake. We installed five permanent GNSS stations in June 2015 and 11 episodic GNSS stations between June and December 2015. Seven of these stations were measured again in November 2016 (Figs. 2 and 3). We analyzed these data together with the continuous GNSS networks established by LDG-DASE, Caltech (www.unavco.org), Central Washington University (http://www.geodesy.cwu.edu) and with data from the GNSS sites defined in the ITRF2014 reference frame (ARTU, BADG,BAKU,BJFS, BJNM, CHUM, CUSV, GUAO, HYDE, IISC, IRKJ, IRKM, KIT3, KUWT, LHAZ, MDVJ, POL2, SGOC, SHAO, TALA, TASH, TCMS, TEHN, TNML, URUM, ZECK).

Commenté [jl3]: Je comprend pas à quoi correspondent ces données, d'où elles proviennent !

The data were analyzed using the Bernese 5.2 software, with absolute antenna phase center offset models, together with precise orbits, earth rotation parameters, ocean tidal loading and atmospheric tidal loading estimates. Velocities and time series were estimated in the ITRF2014 reference frame (Altamimi et al., 2016) with discontinuities associated with this reference frame and expressed in terms of the India fixed reference frame by the use of the rotation pole

Commenté [jl4]: ETRANGE : EST-CE UTILE ? RETIRER OU METTRE UNE REFERENCE ?

proposed by Ader et al. (2012). This rotation pole, originally proposed to describe the motion of India relative to ITRF2005, rather describes accurately the India plate motion in the ITRF2014 reference frame, as shown by Jouanne et al. (2017) and as exemplified by the lack of velocity of the cGPS SIM4 station located on the India plate (Fig. 3),. In any case, the eventual velocities changes introduced by the change of ITRF are negligible compared to the large postseismic displacements.

Commenté [jl5]: Changement entre quoi ? et introduit par qui ?

We followed the resolution strategy with (1) an initial ionosphere-free analysis with calculation of the residuals; (2) a residual analysis; (3) code-based wide-lane ambiguity resolution for all baselines (Melbourne, 1985; Wübbena, 1985), using differential code bias (DCB) files when available and calculation of the ionosphere-free solution with the introduction of resolved Melbourne-Wübbena linear combination ambiguities; (4) phase-based wide-lane (L5) ambiguity resolution for baselines < 200 km and computation of the ionosphere-free solution with the introduction of resolved ambiguities; (5) resolution of the previously unresolved ambiguities for baselines < 2000 km using the quasi ionosphere-free strategy of resolution; (6) direct L1/L2 ambiguity resolution for baselines < 20 km with the introduction of an ionosphere model; (7) calculation of the normal equations; (8) a compatibility test between the daily free solution and ITRF2014 solution, selection of compatible ITRF2014 stations and (9) transformation of the daily normal equation in the ITRF2014 reference frame with a six-parameter Helmert solution (three translation parameters and three rotation parameters) using the ITRF2014 selected stations. During these steps, site-specific troposphere parameters were estimated every two hours.

Normal equations were analyzed together to determine accurate velocities in the ITRF2014 reference frame with the introduction of ITRF2014 coordinates and velocities. Outliers and new discontinuities were detected using the ‘‘Find Outliers and Discontinuities in Time Series” tool in the Bernese 5.2 software that takes annual seasonal fluctuations into account and reduces,

Commenté [jl6]: Plutôt : « simultaneously ?

step by step, the discrepancy between the functional model and the time series due to statistical adjustment (Ostini et al., 2008). As the Bernese 5.2 software underestimates the daily errors given that systematic errors or mismodeled parameters are not included in the formal error (Hugentobler et al., 2001), we rescaled the formal errors by multiplying them by a factor of 10 to obtain a more realistic estimated error.

RESULTS: POSTSEISMIC DISPLACEMENTS AT THE SURFACE.

We consider that displacements contain three superimposed signals: the interseismic displacements, the postseismic displacements and the seasonal signal associated with the loading of the Ganga Plain during the monsoon and its unloading during the dry season (Bettinelli et al., 2008; Fu and Freymueller, 2012; Gualandi et al., 2016). In order to analyze postseismic displacements, we removed the interseismic displacements that were either measured before the Gorkha earthquake for the sites that already existed before this event (BESI, BRN2, CHLM, DAMA, GUMB, KKN4, KLDN, LMJG, NAST, ODRE, RMJT, RMTE, SNDL, SYBC, TPLJ) (Jouanne et al., 2017) or were estimated using interseismic deformation modellings performed by Jouanne et al. (2017) for the new GNSS sites (Fig. 2).

In order to evaluate the seasonal annual components, we analysed the time series between 2000 and April 2015 for the available cGNSS stations (BESI, BRN2, CHLM, DAMA, GUMB, KKN4, KLDN, LMJG, NAST, ODRE, RMJT, RMTE, SNDL, SYBC, TPLJ) using the FODITS program in the Bernese 5.2 software (Ostini et al. 2008). For the cGNSS stations installed after the earthquake, we interpolated in space the values obtained from the cGNSS stations that had been installed for several years to correct the time series for the components of the seasonal signal (annual signal amplitudes and phase difference, Table 1).

Commenté [jl7]: Le critère de choix ou de disponibilité n'est pas clair.

The postseismic displacements for the period when most of the GNSS stations were available (between June 24, 2015 and late 2016) is shown (Fig. 3) to compare site displacement measured during the same time span. Postseismic displacements are characterized by the southward displacements of the points north of the Gorkha rupture (CHLM, GUMB, TSM1). The station that recorded the greatest postseismic displacement is CHLM (Fig. 3) located to the north of the rupture, with 40 mm of southward displacement between April 25 and June 24 and 100 mm of southward displacement between June 24, 2014 and late 2016. The points located in the northern part of the rupture zone (KKN4, GURJ, BALA) are affected by moderate southward postseismic displacements, whereas the points located at the southern end of the rupture, near to and south of Kathmandu (CHIR, DAMA,NAST and XYAK), are affected by a negligible postseismic displacement. It should be noted that the points at the western part of the rupture (LMJG, GORK and ANBU) are not affected by postseismic displacements whereas the points located several kilometers to the east of the April 25, 2015 rupture (CHAR, JIR2, MALU) are affected by significant postseismic displacements reaching 35 mm (Fig. 3). Given that these points were installed after the May 12, 2015 Mw 7.2 main aftershock, these postseismic displacements may be related to the postseismic deformation induced by this earthquake.

Significant postseismic displacements are therefore restricted to the northern part of the rupture zone and to an area to the north of it (Figs. 3 and 4). It is important to note that there are no clear postseismic displacements to the south of the Gorkha earthquake rupture and, like Mencin et al. (2016), we exclude the occurrence of a significant afterslip along the southern part of the MHT. Therefore, the slip deficit along the MHT south of Kathmandu is not resorbed aseismically by a slip along the MHT from the rupture zone to the MFT where the MHT emerges. The slip deficit could then possibly be resorbed by a future large earthquake between the southern end of the rupture near Kathmandu, and the MFT near the Ganga Plain, as has

probably already happened in the 1866 earthquake (Oldham, 1883; Szeliga et al., 2010), or by a larger earthquake rupturing the locked fault zone from the brittle-ductile transition zone to the surface, in a similar way as in the subduction zones (Melnick et al., 2012; Moreno et al., 2012) or to the 1934 Nepal-Bihar earthquake (e.g. Mugnier et al., 2013).

As postseismic deformation is primarily characterized by southward displacements, we illustrate in Figure 4 the postseismic deformation with the time series for the south component corrected for the interseismic component and the seasonal signal in the India fixed reference frame. The time series present a progressive decrease in postseismic displacement with time, which suggests a progressive dissipation of the stress perturbation induced by the earthquake. The CHLM time series presents a jump corresponding to the May 12 Mw 7.2 main aftershocks, whereas the other stations were not significantly affected or were installed too late to record this coseismic displacement. The GUMB and DCN4 station time series present anomalous displacements respectively 340 to 480 days and 420 to 640 days after the main shock. Moreover, the anomaly affecting the GUMB time series, which began respectively in April 2016, cannot be explained by the monsoon that began two months later, whereas the anomaly affecting the DCN4 time series, which began in June 2016 is close to the beginning of the monsoon. We assume that these local variations are induced by local phenomena such as local unstabilities induced by the main shock.

MODELING POSTSEISMIC- DISPLACEMENT.

We have chosen to test the origin of the progressive release using three hypothesis with the Relax 1_0_7 software (Barbot et al., 2009; Barbot and Fialko 2010; Bruhat et al., 2011; Rousset et al., 2012): a postseismic deformation controlled by afterslip, viscous relaxation of the stress perturbation and an association of these two mechanisms.

This software computes the displacement and stress due to dislocations and the nonlinear postseismic time-dependent deformation, the latter either controlled by viscous bodies with

power-law rheology or by rate-strengthening friction faults. This software takes into account gravity and is based on a Fourier-domain elastic Green's function and an equivalent body-force representation of deformation mechanisms.Ce software est appliqué sur un maillage régulier, et dans le cas du seisme de Gorkha, nous avons utile un zone d'étude de 50? km de large sur 70? km de large avec une maille élémentaire de 3? km.

For these modellings, we use the same MHT geometry as the one used for the pre-earthquake deformation (Jouanne et al., 2017) (Fig. 5); this geometry also fits with the location of the rupture zone proposed by Grandin et al. (2016) and in Figure 6. The geometry of the MHT is formed by a succession of flats and ramps characterized by a southern large flat (95-100 km) dipping 7° northward, a crustal ramp dipping 27° northward between 15 and 25 km and a northern flat dipping 7° northward as illustrated by receiver-function data (Duputel et al. 2016).

As postseismic displacements only affected stations north of Kathmandu, postseismic slip along the MHT did not affect all the upper flat of the MHT but only its northern parts. If we consider the points BALE, KKN4 and GURJ (Fig. 3 and 4) that are nearly at the same distance from the upper flat-ramp connection, it appears that the eastern one (BALE) is affected by a more important postseismic displacements than the two others located in the western part of the upper flat of the MHT. We have then considered that these surficial variations of the displacement reflect the afterslip distribution along the MHT. We have considered in our simulation a segment of the upper flat affected by an afterslip wider in the eastern part of the upper flat than in the western part (Fig. 9). Spatial variations in the time series have led us to consider a 25 km wide western segment and a 40 km wide eastern segment and the boundary between these two segments coincides with the western edge of the Mai 12, 2015 rupture and with the Gaurishankar lateral ramp as illustrated in Figure 1. This spatial variation also reflects interseismic coupling variations between the western and eastern parts: the western part was completely locked whereas the eastern part was only partially locked with a coupling of 0.7 (Fig. 8) (Jouanne et al., 2017).

To test the models, we used a time series that was corrected from interseismic velocities and seasonal components. For the GUMB and DCN4 time series, which present an unexpected behavior, we suspect local superficial effects superimposed on postseismic signal; we have therefore chosen to exclude these data from the modeling.

The preferred solutions were selected using the comparison between the observed and simulated time series (Fig. 7) with the estimation of WRMS for each simulation.

Viscous relaxation model.

The estimation of the coupling during the interseismic period (Betinelli et al., 2006; Ader et al., 2012; Jouanne et al., 2017) suggests a ductile behavior along the northern flat of the MHT. We therefore test the hypothesis that postseismic displacements reveal a viscous relaxation of the stress perturbation induced by the main shock and its main aftershocks. The ductile behavior is temperature dependant (Scholz, 1998) and does not occur in the brittle crust. Viscous relaxation is therefore excluded for the upper flat and the ramp characterized by a temperature lower than 375°C (Robert et al., 2011). Hereafter, we assume that the lower flat only accommodates viscous relaxation.

In this simulation, a low viscous body corresponding to the deeper part of the Main Himalayan Thrust is embedded in an elastic half space (Fig. 5a). The parameters to be determined are the viscosity and the thickness of this body. We have chosen to explore the following ranges of values: viscosity of the body from 10^{17} to 10^{19} Pas. and thickness of the body from 0 to 12 km. The WRMS is always greater than 17 mm and no solution is clearly favored amongst the 200?? numerical runs performed to determine the parameter influence and summarized on Figure 7a.

Commenté [jl8]: Une refernce pour justifier ce choix !

Afterslip model.

If the postseismic displacements are controlled by an afterslip induced by the April 25 2015 Mw 7.9 earthquake, these displacements can be simulated by a progressive release of the stress perturbation due to the main shock. We assume that the afterslip takes place (Fig. 5) along the northern part of the upper flat of the MHT affected by the April 25, 2015 earthquake, along the crustal ramp north of the rupture zone and along the lower flat north of this ramp.

We assign rate-strengthening properties derived from laboratory experiments (Dieterich, 1979; Ruina,1983) to these three fault segments with:

$$V = 2\,\dot{\gamma}_0\,\sinh\frac{\Delta\tau}{(a-b)\sigma} \qquad \text{(eq. 1)}$$

Where V is the slip on the fault, Δτ is the stress perturbation induced by the earthquake that is progressively released by the afterslip, $\dot{\gamma}_0$ and (*a* - *b*) are constitutive parameters and σ the stress drop during the earthquake.

The initial stress perturbation associated to the coseismic slip distributions of the April 25, 2015 and May 12, 2015 earthquake estimated by Grandin et al. (2016) (Fig. 6) is calculated with the Relax1_0_7 software.

We explore the parameters space (Fig. 7b) formed by $\dot{\gamma}_0$ (from 50 to 800 mm/year), and the friction along the considered planes (from 0 to 1.2) for an (*a* - *b*) σ values of 45 MPa**.** Amongst the 5000000?? numerical runs performed to determine the parameter influence (Figure 7b), a minimum of 3.9 mm is found for the WRMS (Fig. 7b) linked to friction coefficient and $\dot{\gamma}_0$ of 0.9 and 480, respectively.

Afterslip and viscous relaxation model.

This simulation takes into account the hypothesis that the northern flat may be a zone affected by ductile deformation (e.g. Elliott et al., 2016 VERIFIER) channel (Beaumont et al., 2001),

Commenté [jl9]: VERIFIE :je ne suis pas sur vérifie……

Commenté [jl10]: Quel type de logiciel a utilisé Grandin ? Je suis surpris qu'il n'y ai pas de références concernant le stress drop et la contrainte de Coulomb ?

Commenté [jl11]: Une reference pour justifier ces plages de valeur ?

while the upper part of the MHT is probably in a brittle condition as shown by the high coupling of the upper flat and crustal ramp during the interseismic period (Jouanne et al., 2004; Ader et al., 2012; Jouanne et al., 2017).

We test the hypothesis of a mixed origin for the postseismic deformation (Fig. 5), with a viscous relaxation controlled by a deep low viscosity body centered on the northern MHT flat, as done above, whereas the afterslip occurs along the crustal ramp and the northern part of the southern flat. We adopt, as an a priori model for the afterslip component, the above model that minimizes the WRMS amongst the models uniquely based on afterslip and we have chosen to explore the following parameters: viscosity of the low viscosity body (from 10^{17} to 5.10^{19} Pa.s) and the thickness of this body (0 to 6 km).

Amongst the 50000000000?? numerical runs performed to determine the parameter influence (Figure 7c), a minimum of 4 mm is found for the WRMS (Fig. 7c) linked to a 3 km thickness for the viscous body and a 8.10^{18} Pas viscosity.

DISCUSSION.

Comparison between the different models.

The comparison of the WRMS for the models performed with the three tested hypotheses (Fig. 7?) indicates that the models with only viscous relaxation on the lower flat of the MHT have much higher WRMS and can be excluded.

The two other models, afterslip alone or afterslip associated with a viscous relaxation on the lower flat of the MHT, have WRMS of the same order (smaller than 4 mm) and are not distinguishable; the only noticeable change is obtained for the northern station, CHLM, close to the lower flat (Fig. 8?). The numerical approach modeling therefore does not allow to choose

between the two hypotheses -afterslip alone or afterslip combined with viscous relaxation on the lower flat.

All the retained simulations indicate (Figures 6c): a) a moderate afterslip along a large part of the ramp, b) a significant afterslip along the northern part of the upper flat; c) large afterslip where the coseismic slip gradient was high: at the upper flat/crustal ramp transition, locally in the rupture area and near the southern boundary of the rupture; d) the lack of significant postseismic displacements near most of the southern border of the numerical model on the upper flat segment of the MHT affected by afterslip. Afterslip along the southern part of the upper flat, to the south of the southern border of the numerical model is therefore excluded, as we had *apriori* assumed for the determination of the mesh based on the nearly null postseismic displacement measured south of the Gorkha rupture zone. The models nonetheless indicate a high post seismic displacement at the western edge of the mesh and suggest that post-seismic motion could extend farther west of this zone.

Evolution of the afterslip along the MHT.

The slip velocity evolution through over time and space of our preferred model indicates that (Fig. 9): the lower flat of the MHT is affected by a slow large-scale afterslip decreasing over time, whereas the crustal ramp is affected by a negligible afterslip without significant lateral variations. The northern part of the upper flat is characterized by local patches of high velocity afterslip; the latter reached 2 m/year with a significant lateral variability and a significant decrease between D + 40 days and D + 180 days. The areas of the upper flat affected by significant slip velocity are located close to the flat-ramp transition that corresponds to the northern boundary of the rupture. Areas of the upper flat locally affected by a significant slip velocity are characterized by local high coseismic displacement gradient in Grandin et al.'s model (2016) and then to local high deviatoric stress to be release. Locally, slip also occurred

southward in areas near the southern end of the mesh, upper flat segment of the MHT affected by afterslip.

Our modelling suggests changes of width of the upper flat of the MHT affected by afterslip (Fig. 8). These spatial changes and the significant misfits between observed and simulated time series mainly observed for the JIR2 and GURJ stations may reflect spatial friction coefficient variations not modelled by our simple models.

The afterslip properties along the MHT.

In the Relax software, it is possible to only consider one single afterslip property (friction ratio and constitutive parameters) for all of the fault segments. As a result, we have then considered the same properties for the upper flat, crustal ramp and lower flat of the MHT. Our preferred model that allows a good fit with the observed time series (Fig. 7b?) has been obtained with $\dot{\gamma}_0$ = 450 mm/year and a friction of 0.9 for (a-b) σ = 45 Mpa. The best-fit models consider two distinct parts for the upper flat of the MHT.

DISCUTER CES VALEURS PAR RAPPORT A CE QUI EXISTE DANS LA LITTERATURE ET PAR RAPPORT A DE QUE CES GRANDEURS REPRESENTENT (ELLES N'ONT PAS UNE VALEUR UNIQUEMMENT DANS CE MODELE, ENFIN J ESPERE)

(a-b) σ ? ??????????????????????????????

A friction coefficient of 0.9 would mean a friction angle close to 41° and is very high in respect to the usually inferred values. For example the friction angle was estimated at 20° for the Indian crust in the modeling of Berger et al. (2003). Values greater than 41° were nonetheless found experimentally for numerous rocks (Kulhawi, 1975).

~~The interseismic and postseismic modelings therefore suggest a frictional variation along the upper MHT on both sides of the Gaurishankar lateral ramp~~.

Commenté [M12]: Cette partie est largement une reprise du paragraphe précédent, il faudrait peut-être regrouper

Commenté [jl13]: JE SUIS PAS SUR QUE CA SOIT JUSTE VU QUE TU IMPOSES TA LIMITE AVANT LA MODELISATION ; !

Commenté [jl14]: JE COMPREND PAS CE QUE TU VEUX DIRE

Commenté [jl15]: COMME TU N'INTRODUIT PAS LA RUPTURE DE MAI A L'EST, TU N'AS PAS DE PERTURBATION DES CONTRAINTES A L'EST ET DONC PAS DE POST A L'EST ! PEUT ETRE NE PAS EN PARLER

Viscous relaxation controlled by a low viscosity zone along the lower flat of the MHT.

The time series for the stations located above the rupture zone, or to the south of it, are not correctly simulated by a viscous relaxation controlled by a ductile body centered on the northern flat. In the numerical models where afterslip along the upper parts of the MHT has been introduced, the low viscosity body has to be thin (close to 3 km) to minimize the discard between model and data and in this case the discard is small.

We therefore believe that viscous relaxation controlled by a low viscosity body cannot alone explain the recorded postseismic deformation and another source of deformation located to the south of the deep flat (i.e. afterslip) is needed.

Nonetheless, the low viscosity body is a reasonable assumption as it may control the low coupling along the lower flat documented for the interseismic period (Fig. 8). Furthermore, low viscosity level has been suggested from the interpretation of deep image of the Himalayan crust (e.g. Zhao et al., 1993; Nelson et al., 1996).

A channel flow model (Beaumont et al., 2001) was even proposed to describe the Himalayan tectonics evolution and is based on a very thick ductile zone (more than 10 km thickCONTROLER), so thick that the horizontal velocity depicts a peculiar gradient, with a maximum velocity in the center of the ductile zone. Our results nonetheless suggest that the ductile zone is less than 3(or 5?) km thick beneath the very southern part of the Tibet plateau. Therefore, we suggest that the recent tectonics of Himalaya is not controlled by a channel flow deformation at depth, although our results does not preclude a thicker ductile zone towards the north.

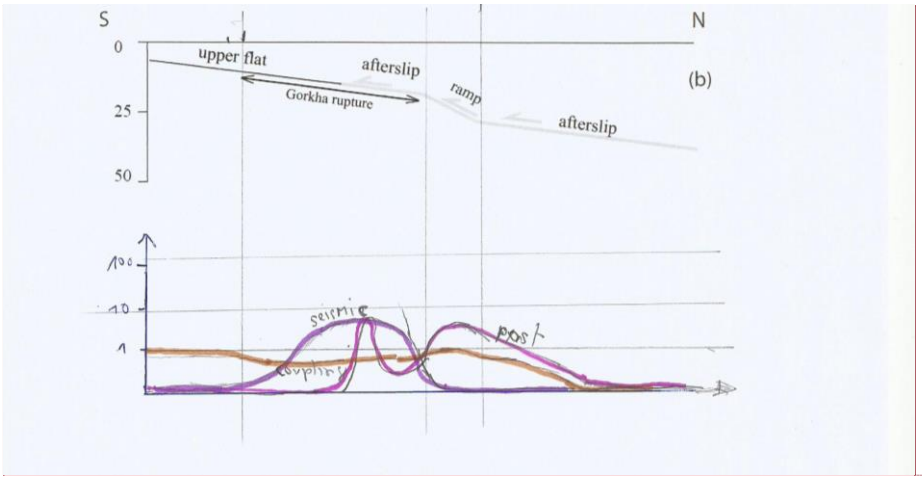

Fig. 10 Comparison between interseismic coupling ratio, seismic slip and afterslip coupling ratio (pour illustrer le paragraphe ci-dessous!). Les valeurs pourraient être prises sur une seule coupe ou correspondre à une moyenne d'un segment de largeur de la rupture, ceci projeté perpendiculairement à la rampe,

Summary

We then interpret our results as (1) a large-scale afterslip or a viscous relaxation of a thin zone (~3 km thick) of high fluidity along the lower flat of the MHT and (2) a moderate afterslip along the crustal ramp that prolongates down-dip the Gorkha rupture as well as (3) a high-velocity small-scale afterslip along the southern boundary of the segment and (4) a high-velocity afterslip in areas characterized by a significant coseismic slip gradient during the earthquake. This pattern where a moderate afterslip along the crustal ramp prolongates down-dip the rupture till the ductile levels as also been shown for the postseismic deformation following the 2005 Balakot-Bagh earthquake (Jouanne et al., 2011; Wang and Fialko, 2014), for the deformation consecutive to the 1995 Chi-Chi earthquake (Yu et al., 2003; Perfettini and Avouac, 2004) and for the 1995 Jalisco earthquake (Hutton et al., 2001).

Commenté [M16]: CETTE FIGURE ME PARAIT INDISPENSABLE POUR SYNTHETISER DE MANIERE ATTRACTIVE TOUT CE TRAVAIL.....

Commenté [M17]: Moi je représenterai bien sur un même diagramme, en dessous de la coupe les mouvements co, post et inter sismique, ce qui permettrai de discuter de la signification du couplage inter-sismique ! Tu montrerai en particulier que toute la zone de rupture n'était pas complétement bloquée

Commenté [jl18]: je comprend pas vraiment le sens de large-scale

Commenté [M19]: Dans ces deux cas on peut estimer un déplacement des compartiments de par et d'autre du MHT ? il faudrait donner des valeurs

CONCLUSION.

The postseismic velocity field clearly shows a lack of displacements to the south of Kathmandu. An afterslip along the southern part of the rupture area of the Gorkha earthquake and along the southern segment of the MHT unaffected by the main shock is then clearly excluded. The slip deficit along the southern part of the upper flat of the MHT, between Kathmandu and the Ganga Plain, would be probably transferred along the MHT by an earthquake of large magnitude, as was possibly the case after the previous 1833 large earthquake along this segment of the MHT: the 1833 earthquake was followed by a second shock in 1866, in the vicinity of Kathmandu, possibly to the south. To the west and east of the Gorkha rupture, postseismic displacements are nearly negligible, and afterslip does not affect the upper flat areas of the MHT to the west of the rupture zone.

The simulation of the time series using the Relax software suggest that the postseismic deformation consecutive to the April 25, 2015 earthquake is controlled by an afterslip along the northern part of the upper flat of the MHT, corresponding to the northern part of the rupture, an afterslip along the crustal ramp and an afterslip or viscous relaxation of thin (~3 km thick) ductile zone along the lower flat of the MHT of Il manque des estimations numériques 200 ? mm dans l'année suivante en moyenne ?. Viscous relaxation along a ductile body centered on the lower flat of the MHT alone cannot explain the postseismic deformation.

Commenté [M20]: Pas si négligeable que ça sur le maillage (coin inférieur gauche !)

Commenté [M21]: Mon problème dans ce papier, c'est que tu regarde un segment du plat supérieur qui comprend aussi le séisme de mai à l'ouest, mais on sait pas si tu en tiens compte dans la modélisation pour le chargement.

Commenté [M22]: Il manque des estimations numériques 100 mm dans l'année suivante en moyenne ?

Commenté [M23]: Il manque des estimations numériques 100 mm dans l'année suivante en moyenne ?

Commenté [M24]:

ACKNOWLEDGMENTS.

The figures and map were prepared using the Generic Mapping Tools software (Wessel and Smith, 1995) and Paraview software (Ahrens et al., 2005; Ayachit, 2015). This material is partially based on data provided by the Nepal permanent GNSS network (DMG, Caltech, DASE) and data services provided by the UNAVCO Facility with support from the National

Commenté [p25]: Pas dans la biblio

Commenté [p26]: Pas dans la biblio

Science Foundation (NSF) and National Aeronautics and Space Administration (NASA) under NSF Cooperative Agreement No. EAR-0735156. Funds have been provided by the Labex OSUG@2020, by INSU-CNRS, by the AAP of Savoie Mont Blanc University by the IRD and by the ANR Bhoutanepal.

Commenté [p27]: ,

REFERENCES

Ader, T., Avouac, J.P., Liu-Zeng, J., Lyon-Caen, H., Bollinger, L., Galetzka, J., Genrich, J., Thomas, M., Chanard, K., Sapkota, S., Rajaure, S., Shrestha, P., Ding, L., Flouzat, M.. 2012. Convergence rate across the Nepal Himalaya and interseismic coupling on the Main Himalayan Thrust: implications. *J. Geophys. Res*. 117, B04403. http://dx.doi.org/10.1029/2011JB009071.

Adhikari, L.B., Gautam, U.P., Bhattarai, M., Kandel, T., Gupta, R.M., Timsina, C., Maharjan, N., Maharjan K., Dahal, T., Hoste-Colomer, R., Cano, Y., Dandine, M., Guilhem, A., Merrer, S., Roudil, P., Bollinger, L., 2015. The aftershock sequence of the April 25 2015 Gorkha-Nepal earthquake. *Geophys. J. Int.* 203, 2119–2124.

Altamimi, Z., Rebischung, P., Métivier, L. and Xavier, C., 2016. ITRF2014: A new release of the International Terrestrial Reference Frame modeling nonlinear station motions, *J. Geophys. Res. Solid Earth*, 121, doi:10.1002/2016JB013098.

Argand, 1924. La tectonique de l'Asie. 104 p. Compte rendu du congrès géologique international (1922). Vaillant-Carmane press (Liege, Belgium).

Avouac, J.P., Bollinger, L., Lavé, J., Cattin, R., Flouzat, M., 2001. Le cycle sismique en Himalaya, *Comptes Rendus de l'Academie de Sciences - Serie IIa: Sciences de la Terre et des Planètes*. doi:10.1016/S1251-8050(01)01573-7

Avouac, J.-P., Meng, L., Wei, S., Wang, T., Ampuero, J.P., 2015. Lower edge of locked Main Himalayan Thrust unzipped by the 2015 Gorkha earthquake. *Nature Geoscience*, ISSN 1752-0894.

Baillard, C., Lyon-Caen, H., Bollinger, L., Rietbrock, A., Letort, J., & Adhikari, L. B., 2017. Automatic analysis of the Gorkha earthquake aftershock sequence: evidences of structurally segmented seismicity. *Geophysical Journal International*, *209*(2), 1111-1125.

Barbot, S., Fialko, Y., 2010. Fourier-domain Green's function for an elastic semi-infinite solid under gravity, with applications to earthquake and volcano deformation, *Geophys. J. Int.*, 182(2), 568–582, doi:10.1111/j.1365- 246X.2010.04655.x.

Barbot, S., Hamiel, Y., Fialko, Y., 2008. Space geodetic investigation of the coseismic and postseismic deformation due to the 2003 Mw 7.2 Altai earthquake: Implications for the local lithospheric rheology, *J. Geophys. Res.*, 113(B03403), doi:10.1029/2007JB005063.

Barbot, S., Fialko, Y., Bock, Y., 2009. Postseismic Deformation due to the Mw 6.0 2004 Parkfield Earthquake: Stress-Driven Creep on a Fault with Spatially Variable Rate-and-State Friction Parameters, *J. Geophys. Res.*, 114(B07405), doi:10.1029/2008JB005748.

Barbot, S., Fialko Y., 2010. A unified continuum representation of postseismic relaxation mechanisms: semianalytic models of afterslip, poroelastic rebound and viscoelastic flow, - *Geophys. J. Int.*, 182(3), 1124–1140, doi:10.1111/j.1365-246X.2010.04678.x.

Beaumont, C., Jamieson, R.A., Nguyen, M.H., Lee, B., 2001. Himalayan tectonics explained by extrusion of a low-viscosity crustal channel coupled to focused surface denudation. *Nature* 414, 738–742.

Bettinelli, P., Avouac, J.P., Flouzat, M., Jouanne, F., Bollinger, L., Willis, P., Chitrakar, G.R., 2006. Plate motion of India and interseismic strain in the Nepal Himalaya from GPS and DORIS measurements. *J. Geod*. http://dx.doi.org/10.1007//s00190-006-0030-3.

Bettinelli, P., Avouac, J.-P., Flouzat, M., Bollinger, L., Ramillien, G., Rajaure, S.,Sapkota, S., 2008. Seasonal variations of seismicity and geodetic strain in the Himalaya induced by surface hydrology. *Earth Planet. Sci. Lett.* 266, 332–344.

Commenté [p28]: Absent du texte

Commenté [p29]: Absent du texte

Berger, A., Jouanne, F., Hassani, R., Mugnier, J.L., 2004. Modelling the spatial distribution of present-day deformation in Nepal: how cylindrical is the Main Himalayan Thrust in Nepal? *Geophys. J. Int.*, 156, 94–114.

Bhattarai, M., Adhikari, L. B., Gautam, U. P., Laurendeau, A., Labonne, C., Hoste-Colomer, R.& Hernandez, B.,2015. Overview of the large 25 April 2015 Gorkha, Nepal, earthquake from accelerometric perspectives. *Seismological Research Letters*, *86*(6), 1540-1548.

Bilham, R., Larson, K., Freymueller, J.Idylhim members (Jouanne, F., Le Fort, P., Leturmy, P., Mugnier, J.L., Gamond, J.F., Glot, J.P., Martinod, J., Chaudury, N.L., Chitrakar, G.R., Gautam, U.P., Koirala, B.P., Pandey, M.R., Ranabhat, R., Sapkota, S.N., Shrestha, P.L., Thakury, M.C., Timilsina, U.R., Tiwari, U.R., Vidal, G., Vigny, C., Galy, A., De Voogd, B.), 1997. GPS measurements of present-day convergence across the Nepal Himalaya. *Nature* 386, 1–94.

Bollinger, L., Sapkota, S. N., Tapponnier, P. , Klinger, Y., Rizza, M. , Van der Woerd, J., Tiwari, D. R., Pandey, R., Bitri, A., Bes de Berc S., 2014. Estimating the return times of great Himalayan earthquakes in eastern Nepal: Evidence from the Patu and Bardibas strands of the Main Frontal Thrust, *J. Geophys. Res. Solid Earth*, 119, doi:10.1002/2014JB010970.

Bruhat L, Barbot S, Avouac JP, 2011. Evidence for postseismic deformation of the lower crust following the 2004 Mw6. 0 Parkfield earthquake, *J. Geophys. Res. Solid Earth*, 116 (B8).

Dieterich, J. H. (1979), Modeling of rock friction: 1. Experimental results and constitutive equations, J. Geophys. Res., 84, 2161−2168.

Duputel, Z., Vergne, J., Rivera, L., Wittlinger, G., Farra, V., Hetényi, G., 2016. The 2015 Gorkha earthquake: a large event illuminating the Main Himalayan Thrust fault. *Geophys. Res. Lett.* 43 (2517–2525), 2016G. http://dx.doi.org/10.1002/L068083.

Elliott, J., Jolivet, R., Gonzalez, P., Avouac, J.P., Hollingsworth, J., Searle, M.P., Stevens, V.L., 2016. Himalayan megathrust geometry and relation to topography revealed by the Gorkha earthquake. Nature Geosci. http://dx.doi.org/10.1038/NGEO2623.

Commenté [p30]: Absent du texte

Fan, W., Shearer, P.M., 2015. Detailed rupture imaging of the 25 April 2015 Nepal earthquake using teleseismic P waves. Geophysical Research Letters doi:10.1002/2015GL064587

Fu, Y., Freymueller, J.T., 2012. Seasonal and long-term vertical deformation in the Nepal Himalaya constrained by GPS and GRACE measurements. *J. Geophys. Res.* 117, B03407. http://dx.doi.org/10.1029/2011JB008925.

Galetzka, J., Avouac, J.-P., Genrich, J.F., Hudnut, K.W., 2015. Slip pulse and resonance of Kathmandu basin during the 2015 Mw 7.8 Gorkha earthquake, Nepal imaged with geodesy. *Science*, ISSN 0036-8075.

Grandin, R., Vallée, M., Satriano, C., Lacassin, R., Klinger, Y., Simoes, M., Bollinger, L., 2015. Rupture process of the Mw = 7.9 2015 Gorkha earthquake (Nepal):http://dx.doi.org/10.1016/j.jseaes.2016.05.028 insights into Himalayan megathrust segmentation. *Geophys. Res. Lett.* 42 (20), 8373–8382.

Gualandi, A., Avouac, J. P., Galetzka, J., Genrich, J. F., Blewitt, G., Adhikari, L. B., & Liu-Zeng, J., 2016. Pre-and postseismic deformation related to the 2015, Mw7. 8 Gorkha earthquake, Nepal. *Tectonophysics*, DOI: 10.1016/j.tecto.2016.06.014.

Hubbard, J., Almeida, R., Foster, A., Sapkota, S. N., Bürgi, P., & Tapponnier, P., 2016. Structural segmentation controlled the 2015 Mw 7.8 Gorkha earthquake rupture in Nepal. *Geology*, *44*(8), 639-642.

Hugentobler U., Schaer S., Fridez, P., Bernese GPS Software Version 4.2, Astronomical Institute, University of Berne, Switzerland, 2001.

Jouanne, F., Mugnier, J.L., Pandey, M., Gamond, J.F., Le Fort, P., Serrurier, L., Vigny, C., Avouac, J.-P., 1999. Oblique convergence in the Himalayas of western Nepal deduced from preliminary results of GPS measurements. *Geophys. Res. Lett.* 26 (13), 1933–1936.

Jouanne, F., Mugnier, J.L., Gamond, J.F., Le Fort, P., Pandey, M., Bollinger, L., Flouzat, M., Avouac, J.P., 2004. Current shortening across the Himalayas of Nepal. *Geophys. J. Int.* ,157, 1–14.

Commenté [p31]: Absent du texte

Commenté [p32]: Absent du texte

Jouanne, F., A. Awan, A. Madji, A. Pêcher, M. Latif, A. Kausar, J. L. Mugnier, I. Khan, and N. A. Khan, 2011. Postseismic deformation in Pakistan after the 8 October 2005 earthquake: Evidence of afterslip along a flat north of the Balakot-Bagh Thrust, *J. Geophys. Res.*, **116**, B07401, doi:10.1029/2010JB007903.

Jouanne F, Awan A, Pêcher A, Kausar A, Mugnier JL, Khan I, NA Khan, Van Melle J., 2014. Present-day deformation of northern Pakistan from Salt Ranges to Karakorum Ranges, *J. Geophys. Res. Solid Earth*, 119 (3), 2487-2503.

Jouanne F., Mugnier J.L., Sapkota S. N., Bascou B., Pecher A., 2017. Estimation of coupling along the Main Himalayan Thrust in the central Himalaya, *Journal of Asian earth sciences*, January 2017.

Kayal, J.R., 2008. Microearthquake Seismology and Seismotectonics of South Asia. http://dx.doi.org/10.1007/978-1-4020-8180-4.

Kulhawy, F.H. (1975). Stress deformation properties of rock and rock discontinuities. Engineering Geology, Vol. 9, pp 327-350.

Kumar A., Singh SK, Mitra S, Priestley K.F., Shankar Dayal , 2017. The 2015 April 25 Gorkha (Nepal) earthquake and its aftershocks: implications for lateral heterogeneity on the Main Himalayan Thrust, *Geophys. J. Int.*, 208 (2): 992-1008.

Hutton, W., DeMets, C., Sánchez ,O., Suárez, G., Stock, J., 2001. Slip dynamics during and after the 9 October 1995 Mw = 8.0 Colima-Jalisco, Mexico, *Geophys. J. Int.*, 146, 637–658, doi:10.1046/j.1365- 246X.2001.00472.x.

Lindsey, E.O., Natsuaki, R., Xu, X., Shimada, M., Hashimoto, M., Melgar, D., Sandwell, D.T., 2015. Line-of-sight displacement from ALOS-2 interferometry: Mw 7.8 Gorkha Earthquake and Mw 7.3 aftershock. Geophysical Research Letters 42, 6655–6661. doi:10.1002/2015GL065385.

Commenté [p33]: Absent du texte

Melbourne, W.G., 1985. The case for ranging in GPS based geodetic system. Paper Presented at 1st International Symposium on Precise Positioning with the Global Positioning System, Int. Assoc. of Geod., Rockville, Md.

Melnick, D, Moreno, M., Cisternas, M., Tassara, A , 2012. Darwin seismic gap closed by the 2010 Maule earthquake. *Andean Geology*, v. 39, no. 3, p. 558-563.

Mencin, D., Bendick, R., Upreti, B. N., Adhikari, D. P. Gajurel, A. P., Bhattarai, R. R., Shrestha, H. R., Bhattarai, T. N., Manandhar, N., Galetzka, J., Knappe, E., Pratt-Sitaula, B., Aoudia A. & Bilham R., 2016. Himalayan strain reservoir inferred from limited afterslip following the Gorkha earthquake. *Nature Geoscience* , 9, 533–537. doi:10.1038/ngeo2734

Moreno, M., Melnick, D., Rosenau, M., Baez, J., Klotz, J., Oncken, O., Tassara, A., Chen, J., Bataille, K., Bevis, M., Socquet, A., Bolte, J., Vigny, C., Brooks, B., Ryder, I., Grund, V. Smalley, B., Carrizo, D., Bartsch, M., Hase, H. , 2012, Toward understanding tectonic control on the M w 8.8 2010 Maule Chile earthquake. Earth and Planetary Science Letters, v. 321-322, p. 152-165.

Mugnier, J.L., Huyghe, P., Leturmy, P., Jouanne, F., 2004. Episodicity rates of thrust sheet motion in the Himalayas (western Nepal). *In: McClay, K. (Ed.), Thrust Tectonics and Hydrocarbon Systems, vol. 82. A.A.P.G. Memoir*, pp. 91–114.

Mugnier, J.L., Huyghe, P., Gajurel, A., Upreti, B.N., Jouanne, F., 2011. Seismites in the Kathmandu valley and seismic hazard in central Himalaya. *Tectonophysics*. http://dx.doi.org/10.1016/j.tecto.2011.05.012.

Mugnier, J.L., Gajurel, A., Huyghe, P., Jouanne, F., Upreti, B.N., 2013. Structural interpretation of the great earthquakes of the last millennium in Central Himalaya. *Earth Sci. Rev*. 127, 30–47. http://dx.doi.org/10.1016/j. earscirev.2013.09.003.

Mugnier J.-L., Jouanne F., Bhattarai R., Cortes-Aranda J., Gajurel A., Leturmy P., Robert X., Upreti B., Vassallo R.. , 2017. Segmentation of the Himalayan megathrust around the Gorkha earthquake (25 April 2015) in Nepal. *Journal of Asian Earth Sciences*.

Commenté [p34]: déplacé

Commenté [p35]: absent du texte

Nelson K. and 26 others., 1996. Partially Molten Middle Crust Beneath Southern Tibet: Synthesis of Project INDEPTH Results. *Science*, 274, 1684-1687

Oldham, T., 1883. A catalogue of Indian earthquakes from the earliest time to the end of 1869 AD. *Mem. Geol. Survey India* 1, 163–215.

Ostini, L., Dach, R., Meindl, M., Schaer, S., Hugentobler, U., 2008. FODITS: a new tool of the Bernese GPS software. In: Torres, J.A., Hornik, H. (Eds.), *Proceedings of EUREF 2008 Symposium*, Brussels, Belgium.

Perfettini, H., Avouac, J. - P., 2004. Postseismic relaxation driven by brittle creep: A possible mechanism to reconcile geodetic measurements and the decay rate of aftershocks, application to the Chi-Chi earthquake, Taiwan, *J. Geophys. Res*., 109, B02304, doi:10.1029/2003JB002488.

Robert, X., Van Der Beek, P., Braun, J., Perry, C., Mugnier, J.L., 2011. Control of detachment geometry on lateral variations in exhumation rates in the Himalaya: Insights from low-temperature thermochronology and numerical modeling. Journal Geophysical Research Solid Earth 116, 1–22. doi:10.1029/2010JB007893

Rousset,, B., Barbot, S., Avouac J.P0, Hsu, Y.J., 2012. Postseismic deformation following the 1999 Chi-Chi earthquake, Taiwan: Implication for lower-crust rheology, *J. Geophys. Res: Solid Earth*, 117 (B12).

Ruina, A. L. (1983), Slip instability and state variable friction laws, J. Geophys. Res., 88, 10,359–10,370.

Scholz, C.H., 1998. Earthquakes and friction laws. Nature 391, 37– 42.

Szeliga, W., Hough, S., Martin, S., Bilham, R., 2010. Intensity, magnitude, location, and attenuation in India for felt earthquakes since 1762. *Bull. Seismol. Soc. Am*. 100, 570–584. http://dx.doi.org/10.1785/0120080329.

Wang, K., Fialko, Y., 2014. Space geodetic observations and models of postseismic deformation due to the 2005 M7.6 Kashmir (Pakistan) earthquake, *J. Geophys. Res*., 119, 7306-7318.

Wübbena, G., 1985. Software developments for geodetic positioning with GPS using TI4100 code and carrier measurements. Paper Presented at 1st International Symposium on Precise Positioning with the Global Positioning System, *Int. Assoc. of Geod*., Rockville, Md.

Yu, S.-B., Y.-J. Hsu, L.-C. Kuo, H.-Y. Chen, and C.-C. Liu, 2003. GPS measurement of postseismic deformation following the 1999 Chi-Chi, Taiwan, earthquake, *J. Geophys. Res*., 108(B11), 2520, doi:10.1029/2003JB002396.

Zhao, W., Nelson, K.D., Che, J., Quo, J., Lu, D., Wu, C., Liu, X., 1993. Deep seismic reflection evidence for continental underthrusting beneath southern Tibet. *Nature*, 366, 555–559.

Commenté [p36]: Absent du texte

cGNSS Stations	Amplitude of the seasonal component in mm	Phase difference in days	cGNSS stations installed after the Gorkha earthquake	Interpolated amplitude values for the seasonal component in mm	Interpolated phase difference values in days
BESI	1.66	154.50	BALE	1.71	107.96
BRN2	0.95	98.29	BHAZ	1.96	70.64
CHLM	2.81	95.05	CHAR	1.56	115.30
DAMA	2.03	121.64	DNC4	2.37	78.93
GUMB	3.75	103.16	GUMB	1.88	98.56
KKN4	1.60	75.06	GURJ	1.62	74.39
KLDN	1.52	109.80	JIR2	1.50	115.64
LMJG	2.00	102.70	SLBL	1.70	119.67
NAST	1.96	120.66	TSM1	2.62	142.31
ODRE	1.60	107.24	XBAR	1.70	106.86
RMJT	1.14	93.10			
RMTE	0.76	139.44			
SNDL	1.42	127.03			
SYBC	1.42	130.12			
TPLJ	2.03	95.93			

Table 1. Seasonal components affecting the south component of the time series. These values were estimated by FODITS, Bernese 5.2 software (Ostini et al., 2008) for the cGNSS stations that were installed several years before the Gorkha earthquake or interpolated using the values previously estimated for the stations installed after the Gorkha earthquake.

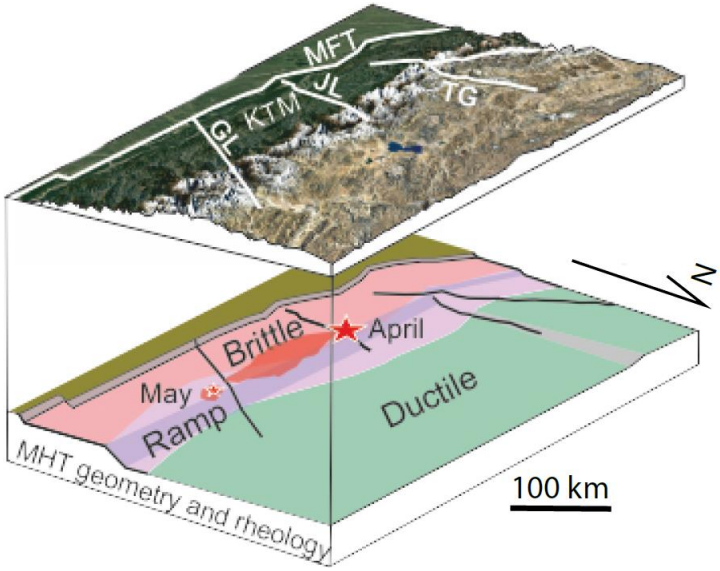

Figure 1. Location of the Gorkha earthquake along the upper flat of the MHT. Heavy purple for ramp geometry; pink, light purple and green for fully locked, partial coupled and ductile MHT, respectivelly; red for rupture zones. The rupture area is bounded by lateral ramps

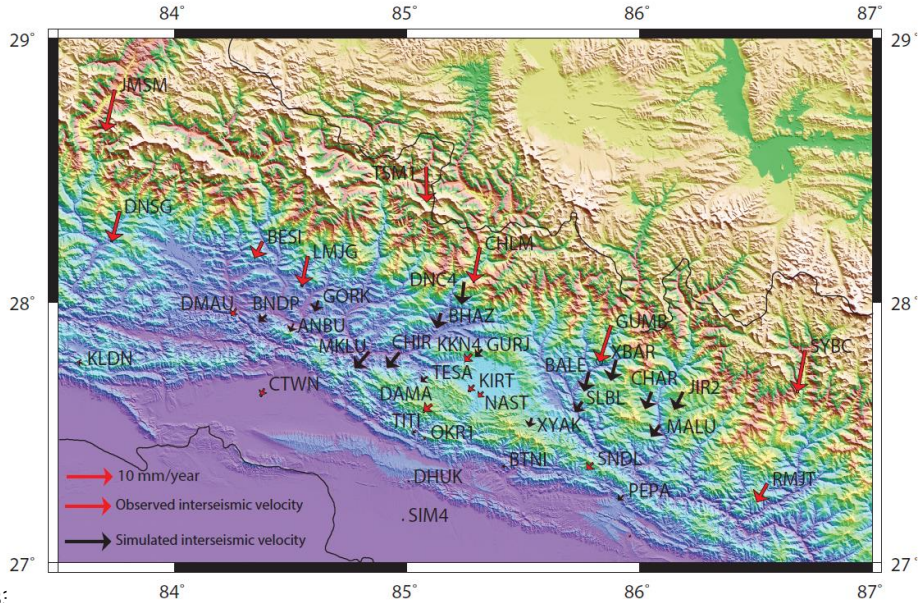

Figure 2. Observed (Jouanne et al., 2017) and simulated interseismic velocities using the model proposed by Jouanne et al. (2017). Velocities are expressed in the India fixed reference frame.

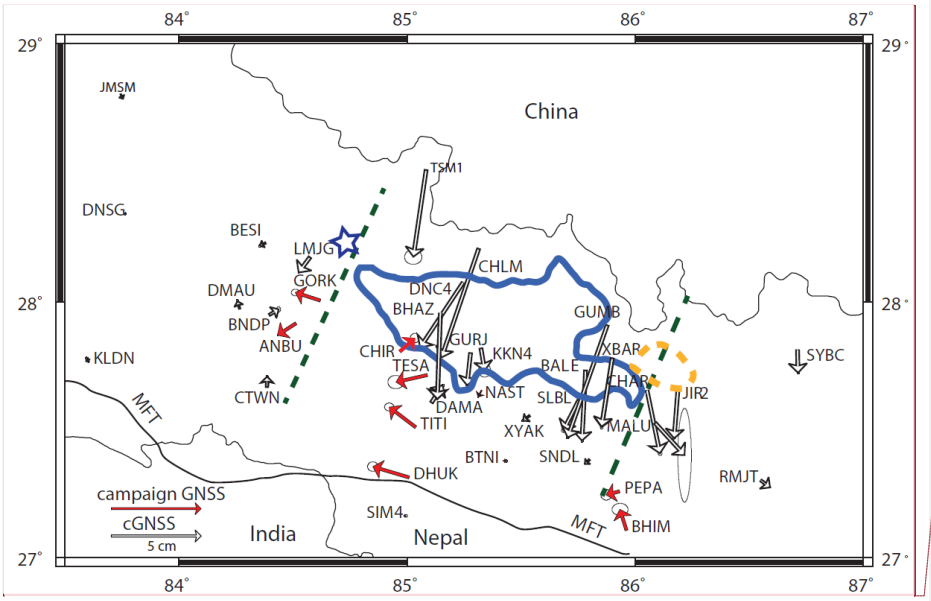

Figure 3. Postseismic displacements following the Gorkha earthquake for the June 24, 2015-December 2016 period. The recorded displacements are corrected for interseismic displacements.
The rupture of the Gorkha earthquake is indicated by a blue line and the rupture of its main aftershocks, on May 12, 2016, is drawn with an orange line. *The star indicates the nucleation of the Gorkha earthquake to the west of its rupture. The dashed green lines indicate the location of the Judi lineament (Kayal, 2008) that separates the main rupture zone from the nucleation area (Kumar et al., 2017) and, on the eastern side, the Gaurishankar lineament (Mugnier et al., 2017). Errors ellipses are drawn for a 95% confidence level.*

Commenté [M37]: La position des deux linéaments est assez piffométrique : regarde plutôt notre article de 2017 !

Commenté [M38]:

Commenté [M39]: Il faudrait mettre quelques lignes d'isovaleurs du glissement (et indiquer la valeur retenue pour les lignes jaunes et bleues

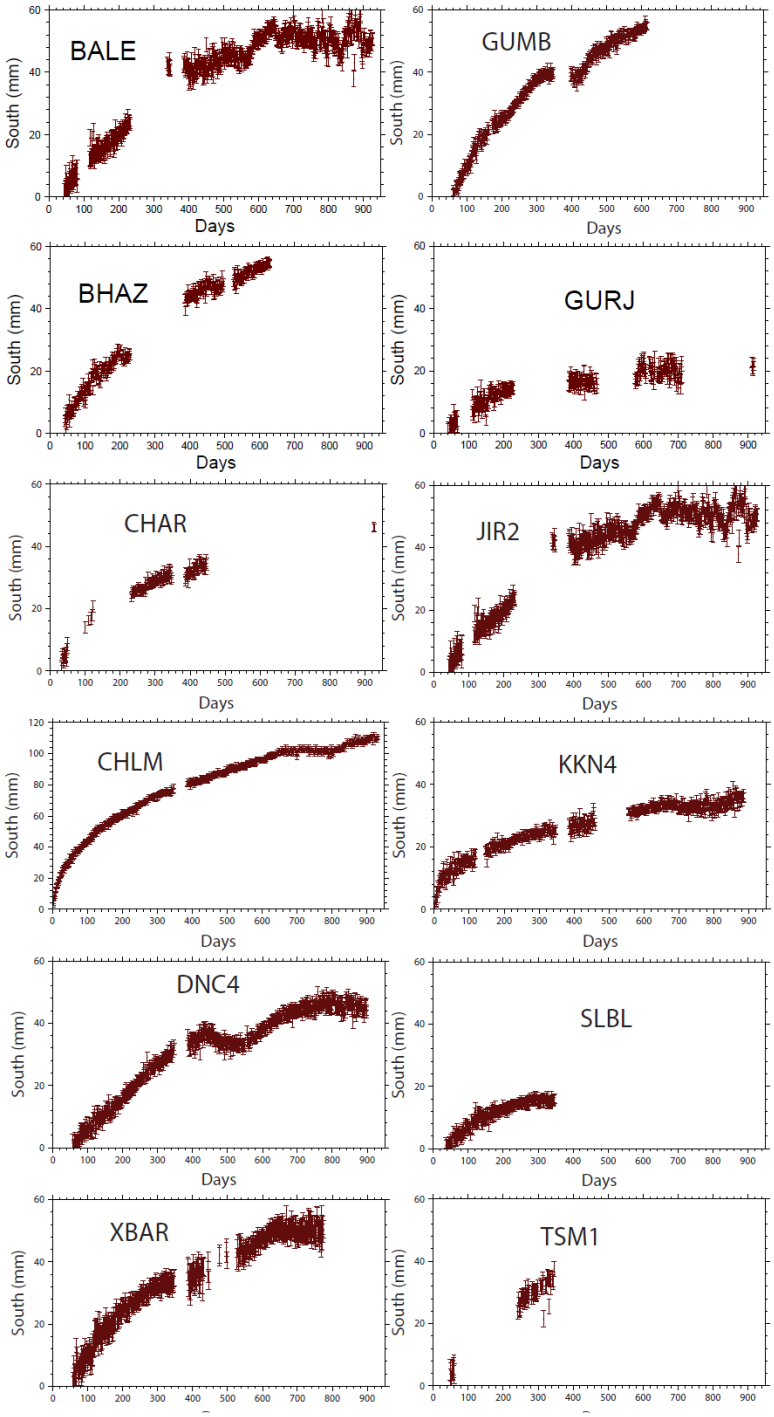
BALE
GUMB
BHAZ
GURJ
CHAR
JIR2
CHLM
KKN4
DNC4
SLBL
XBAR
TSM1
South (mm)
Days

Figure 4. South components for the cGNSS station displacements, corrected from interseismic velocities and seasonal signals estimated during the period before the main shock or extrapolated for the new stations. The locations of cGNSS stations are indicated on Figure 2.

Commenté [jl40]: CETTE FIGURE EST PROCHE DE LA FIGURE 37B3 : LA seule difference, c'est les deux stations non modélisées et l'absence des courbes modélises : pourquoi ne pas faire une seule figure ? (Enfin je comprens l'idee de séparer donnees et resultat du modele..°

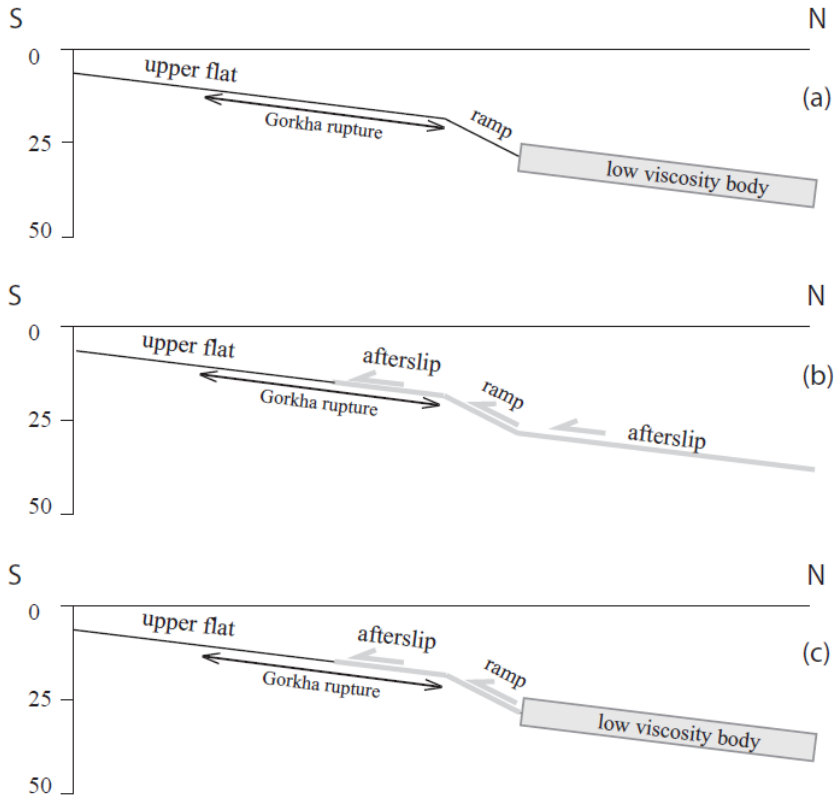

Figure 5. Geometry and rheological properties considered in the numerical simulations of postseismic deformation. (a) Viscous relaxation controlled by a high fluidity body embedded in a half-space characterized by a low fluidity, (b) afterslip along the northern part of the upper flat of the MHT, along the ramp, and along the lower flat of the MHT and (c) viscous relaxation controlled by a high fluidity body embedded in a half-space characterized by a low fluidity and afterslip along the crustal ramp and along the northern part of the upper flat.

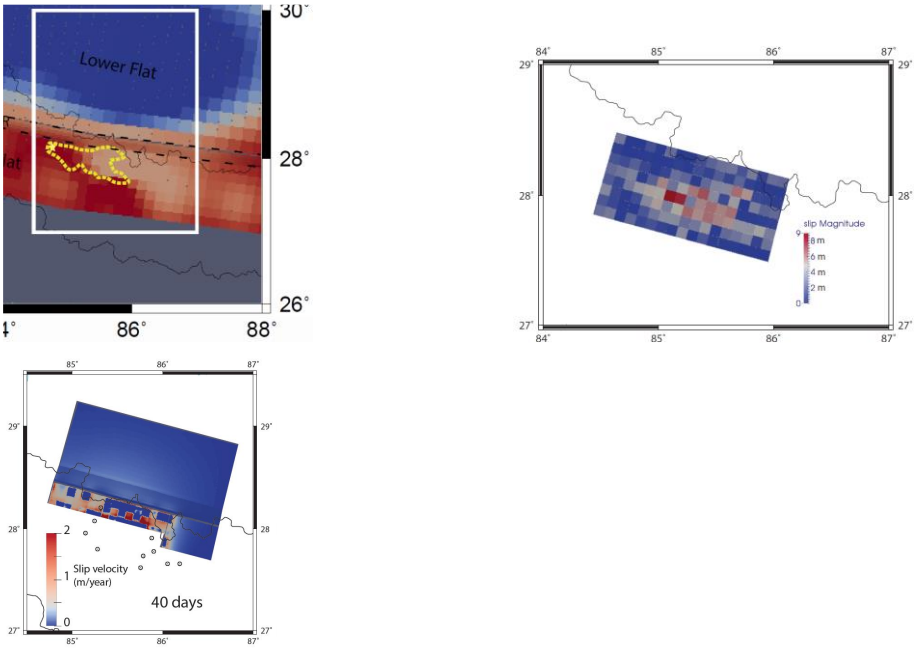

Figure 6. Description of the inter and co-seismic and post deformation on the 3 ? km mesh used for the modeling of the deformation with the Relax software. a) Coupling along the Main Himalayan Thrust during the interseimic period (before the Gorkha earthquake) (modified from Jouanne et al., 2017). The white rectangle indicates the location of Figure 9. CR indicates the location of the crustal ramp. b) Coseismic slip distribution (adapted from Grandin et al., 2016), and used as input for our numerical simulation. c) an example of the post-seismic deformation (PAR EXEMPLE TU DEVRAIS PRESENTER LE DEPLACEMENT POSTSEISMIQUE CUMULE POUR preferred afterslip model ET TU DEVRAIS PLACER SUR TOUTES CES FIGURES LE TRACE DE LA RUPTURE DE AVRIL et CELLE DE MAI

Commenté [jl41]: Représenter la limite de la rupture par une ligne par dessus

Commenté [M42]: *: le décallage du maillage au front correspond tres bien avec la terminaison sud de la rupture de Mai! Ca permetrai de visualizer tout cela*

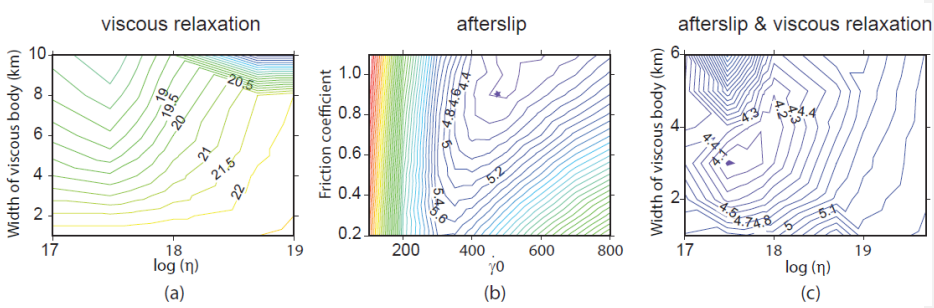

Figure 7. Research of the best solution, with the plot of the WRMS, for (a) the viscous relaxation hypothesis controlled by a viscous body along the lower flat of the MHT, (b) afterslip hypothesis and (c) afterslip and viscous relaxation controlled by a viscous body along the lower flat of the MHT. The best solution for the afterslip hypothesis is indicated by a star, and by a polygon for the afterslip & viscous relaxation.

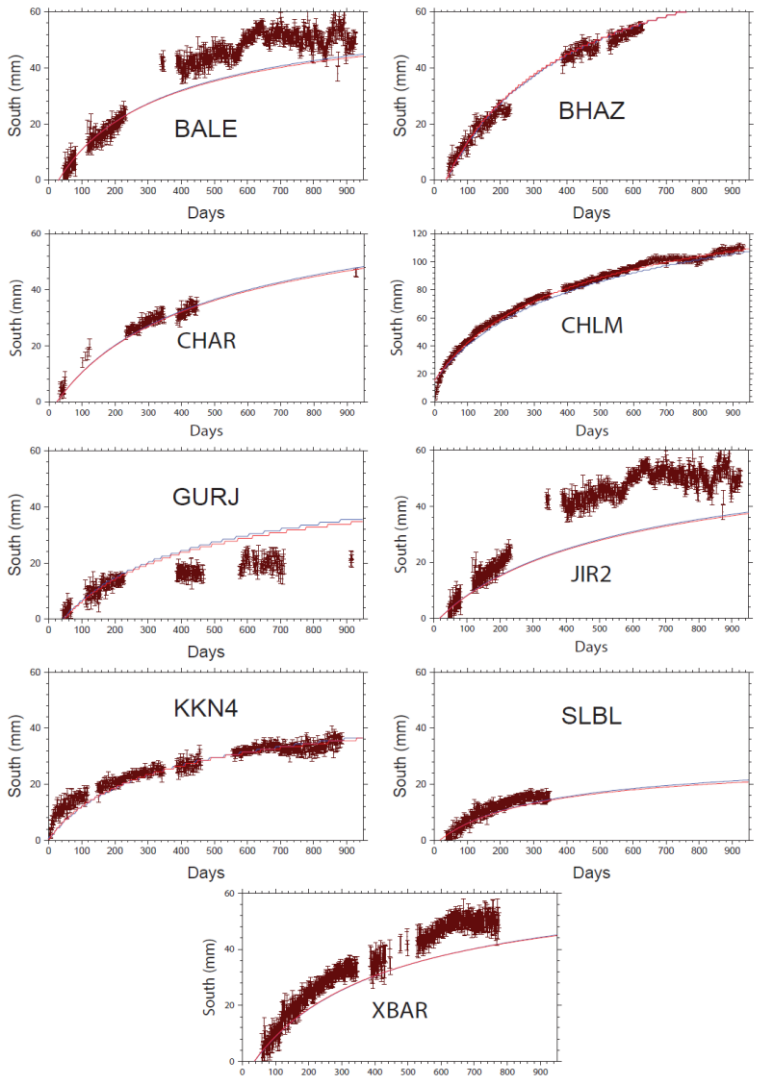

Figure 8. Observed and simulated postseismic time series with our preferred afterslip model, the afterslip & viscous relaxation model and the viscous relaxation model. The simulated time

series with our preferred afterslip and afterslip & viscous relaxation almost always become confused. Blue curve: afterslip hypothesis, red curve: afterslip and viscous relaxation controlled by a viscous body along the lower flat of the MHT. PROCHE DE LA FIGURE 4!

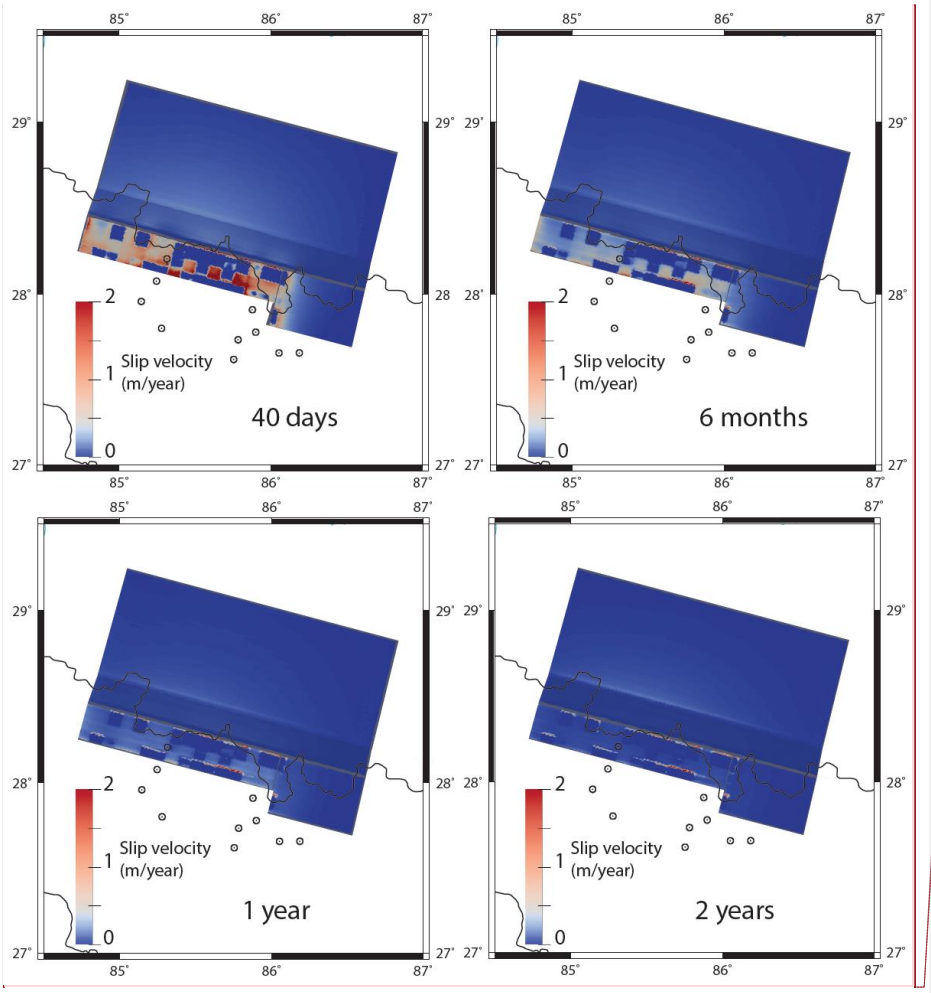

Figure 9. Evolution over time and space of the slip velocity, predicted by our preferred afterslip model, expressed for select data from 0 +40 days to 0 +2 years, the velocity is expressed in

Commenté [M43]: Je sais pas si ton échelle de couleur est bien choisi : presque tout est bleu ???

Commenté [M44]: IL FAUDRAITINDIQUER SUR CETTE FIGURE OU SE SITUE LA RAMPE

Commenté [M45]: Les localisations des sites sont difficiles à voir !

Commenté [M46]: JE comprends pas ce que ça veut dire

meters per year. The locations of the permanent GNSS stations used to constrain our modellings are indicated by open circles.